Chapter 15
Targeted ^{13}C-Labeled Tracer Fate Associations for Drug Efficacy Testing in Cancer

László G. Boros, Richard D. Beger, Emmanuelle J. Meuillet, Jerry R. Colca, Sándor Szalma, Patricia A. Thompson, László Dux, Gyula Farkas Jr., and Gábor Somlyai

L.G. Boros (✉)
Department of Pediatrics, Harbor-UCLA Medical Center, Torrance, CA, USA

SIDMAP, LLC, 2990 South Sepulveda Blvd., Suite 300-B, Los Angeles, CA 90064, USA

Los Angeles Biomedical Research Institute, LABIOMED, Torrance, CA, USA
e-mail: lboros@sidmap.com

R.D. Beger
Division of Systems Biology, National Center for Toxicological Research (NCTR), Food and Drug Administration, Jefferson, AR, USA

E.J. Meuillet
The University of Arizona Cancer Center, Tucson, AZ 5724, USA

Department of Nutritional Sciences, The University of Arizona, Tucson, AZ, USA

J.R. Colca
Metabolic Solutions Development Co., Kalamazoo, MI, USA

S. Szalma
MeTa Informatics, San Diego, CA, USA

P.A. Thompson
The University of Arizona Cancer Center, Tucson, AZ 5724, USA

L. Dux
Department of Biochemistry, Albert Szent-Györgyi Medical Center, University of Szeged, Szeged, Hungary

G. Farkas Jr.
Department of Surgery, Albert Szent-Györgyi Medical Center, University of Szeged, Szeged, Hungary

G. Somlyai
HYD, LLC, Budapest, Hungary

S. Mazurek, M. Shoshan (eds.), *Tumor Cell Metabolism*,
DOI 10.1007/978-3-7091-1824-5_15

Contents

A significantly lower risk of liver cancer incidence was reported for the use of rosiglitazone (odds ratio: 0.73, 95 % confidence interval: 0.65–0.81) in a large population study in patients with type 2 diabetes mellitus (Chang et al. 2012). The protective effects were stronger for higher cumulative dosage and longer duration. In an in vitro efficacy study, we reported that in primary human hepatocellular cells (epithelial; HepG2), the selective peroxisome proliferator-activated receptor (PPARγ-)binding ligand, rosiglitazone, increases fatty acid oxidation (β carbon) and thus ^{13}C-stearate-derived acetyl-CoA exchange (^{13}C labeling) between the extracellular [U-$^{13}C_{18}$]-stearic acid and intracellular carbohydrate [3,4-$^{13}C_2$]-D-ribose pool (RNA). This rosiglitazone efficacy marker demonstrating the flow of carbons from the tracer substrate to product is depicted in Fig. 15.1, while additional details of methods and results are described in a dose-escalating thiazolidinedione efficacy study (Harrigan et al. 2006).

Close examination of the [U-$^{13}C_{18}$]-stearate-derived metabolome (Fig. 15.2; *EZ*Top[U-$^{13}C_{18}$]-stearate) shows a decrease in intracellular [U-$^{13}C_{18}$]-stearate (tracer) content in response to increased (10 μM) rosiglitazone treatment in HepG2 cells. In other words, rosiglitazone undesirably decreases ^{13}C-stearate uptake in HepG2 cells from the media at the expense of mobilizing and synthesizing an unlabeled intracellular pool. This is indicated by the significant >5 % decrease in ^{13}C-labeled intracellular stearate fractions (Fig. 15.2, pellet ^{13}C-stearate panel 107 and 108) after rosiglitazone treatment (see also Table 15.1, pellet stearate panel 107, 108, significant decrease in comparison with a 1 μM dose).

Nevertheless, as expected, rosiglitazone readily increases tracer stearate oxidation (β carbon) as seen by glutamate, lactate, and ribose labeling on the respective $M_2/\Sigma M$ positions (isobolome-wide acetate-dependent ($n = 9$) labeling after [U-$^{13}C_{18}$]-stearic acid's oxidation (supplied in media), Fig. 15.3; for enzyme and metabolite identifiers, please see Tables 15.3 and 15.4, respectively). However, the negative correlation coefficients between rosiglitazone dosing and ^{13}C-labeled stearate indicate the mobilization and synthesis of stearic acid from an unlabeled substrate pool, which necessitate the evaluation of additional tracer approaches for rosiglitazone efficacy testing in HepG2 cells.

Advancements in stable ^{13}C isotope biological chemistry demonstrate that [1,2-$^{13}C_2$]-D-glucose provides the most precise estimates for glycolysis, the pentose phosphate pathway, and the overall metabolic network (Metallo et al. 2009).

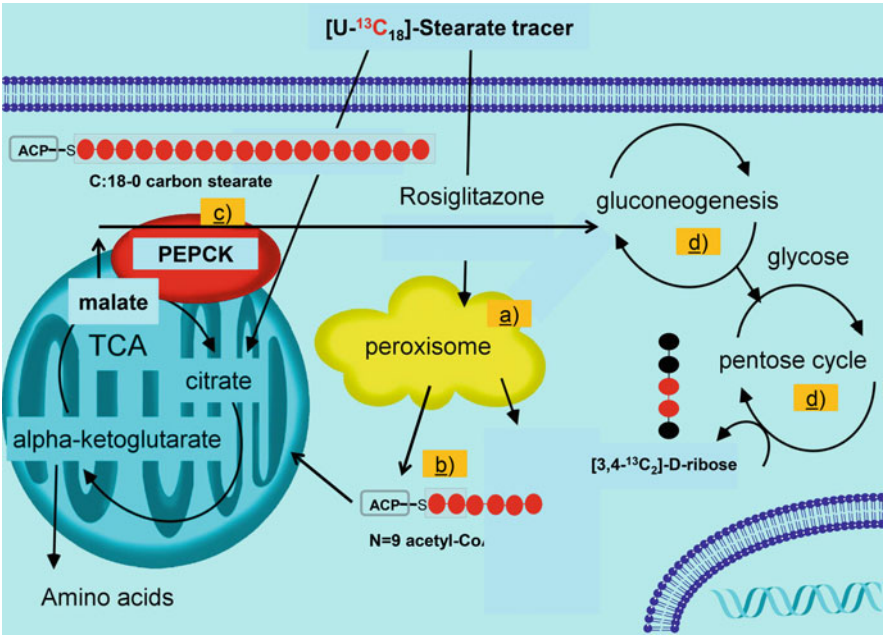

Fig. 15.1 Extracellular [U-$^{13}C_{18}$]-stearic acid tracer substrate entry and its metabolic hubs by rosiglitazone action in HepG2 cells. (**a**) Rosiglitazone increases peroxisomal long-chain fatty acid degradation while shifting, (**b**) acetyl-CoA flux via, (**c**) malate shuttling towards, (**d**) triose, as well as [3,4-$^{13}C_2$]-D-pentose and hexose labeling. Rosiglitazone also forces long-chain fatty acid oxidation to occur in the mitochondria and acetyl-CoA disposal via glutamate synthesis as well as malate shuttling to label RNA ribose and lactate. Please note that acetyl-CoA used by citrate synthase is indistinguishable, if it was generated after peroxisomal chain shortening and mitochondrial fatty acid β carbon oxidation. Increased ribose, lactate, and glutamate labeling after a stepwise rosiglitazone dosing are used as efficacy markers to visualize, via regression analysis, ^{13}C tracer fate associations in HepG2 cells

Because diverse ^{13}C tracer substrate methods are increasingly used in phenotype and drug development (Walther et al. 2012; Mullen et al. 2011; Son et al. 2013; Holleran et al. 1995), our observation of decreased ^{13}C-stearate uptake in a thiazolidinedione efficacy study generates the hypothesis that metabolic tracers, or their mixtures, should only be used with the utmost care as interchangeable efficacy tools, particularly in drug studies. We herein demonstrate a single ^{13}C-glucose tracer as the widely distributed and more precise substrate for cellular carbon metabolism for efficacy testing using the drug-responsive tracer fate regression statistics method among multiple products (Beger et al. 2009). The single [1,2-$^{13}C_2$]-D-glucose tracer generates the standard isotope-dependent targeted cross-labeled ^{13}C-stearate tracer fate metabolomics, which may be the desired approach for drug efficacy testing. Rosiglitazone-induced cross-labeled stearic acid oxidation can label RNA ribose on the recycled acetate-hosting carbon positions, as shown in Fig. 15.4.

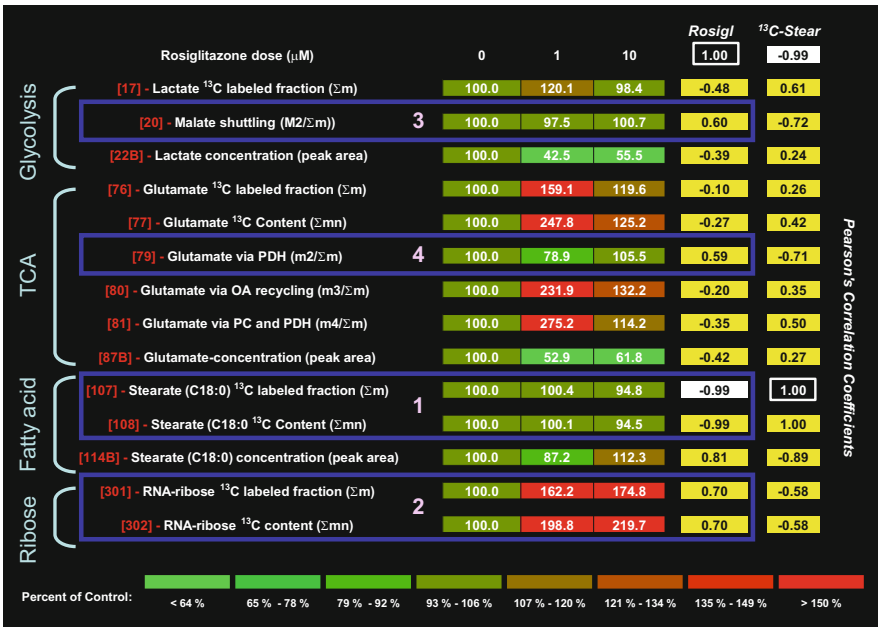

Fig. 15.2 EZTopolome (EZTop([U-$^{13}C_{18}$]-stearate) of in vitro grown HepG2 liver cells, which serves as the color-assisted visual isotopolome matrix screening tool. The EZTop shows decreased stearate tracer uptake (shown in *blue box* 1—line 107, line 108), while stearate concentration increases (line 114B) from unlabeled intracellular pools. Despite decreased tracer uptake, rosiglitazone increases ^{13}C-stearate carbon oxidation and labeling in RNA-derived ribose (shown in *blue box* 2—line 301, line 302) via exclusive malate shuttling as shown in *blue box* 3—^{13}C M_2-labeled lactate; line 20—or glutamate within the cycle by labeling glutamate on C4–C5 positions (shown in *blue box* 4—line 79). The ^{13}C-stearate *EZ*Topolome returns correlation coefficients between rosiglitazone dosing (*Rosigl* column, *yellow*) or ^{13}C-labeled stearate (*^{13}C-Stear* column, *yellow*) as reference variables (*white boxes* = 1) and the rest of the [U-$^{13}C_{18}$]-stearate isotopolome. One can determine the relationship (associations) between rosiglitazone dosing (Rosigl column) and that with ^{13}C-stearate uptake (^{13}C-Stear column), followed by its oxidation in the isotopolome, respectively. Reference ranges are shown with the *white-squared boxes* and regression coefficient of 1.00 with the *black background*

To this effect, [1,2-$^{13}C_2$]-D-glucose EZTopolome (Fig. 15.5; see also Table 15.2) reveals a dose-dependent increase by rosiglitazone on stearate oxidation. The key event in the drug-treated metabolome is the well-maintained glucose tracer uptake with unaltered glycolysis and intracellular stearic acid labeling from glucose, which replaces external stearic acid transport. Glutamate ^{13}C labeling shows much improved correlation coefficients with cross-labeled stearate fractions, and, as expected, rosiglitazone increases RNA-derived ribose labeling, where correlation coefficients are close to one with cross-labeled intracellular stearate as the reference range.

Regression analysis syntax ranges investigate the dependence (dependent or response variables) of all product isotopomers in a heat map format (EZTopolome;

Table 15.1 Targeted ^{13}C isotopolome (^{13}C-labeled metabolome) matrix of rosiglitazone-treated HepG2 (primary hepatocellular carcinoma) cells using [U-$^{13}C_{18}$]-stearate as the single tracer and GC-MS in 72 h cultures. Controls are HepG2 cells treated with 10 % DMSO. N = 3, average (±SD)

Metabolite (source-data-matrix-file-log)	Isotopomer fragment dimension	HepG2 (10 % DMSO)	HepG2 (1 μM Rosiglit)	HepG2 (10 μM Rosiglit)
Lactate (media-CAS: 50-21-5; 17)	^{13}C-labeled fraction (Σm)	0.68 (±0.0388)	0.82 (±0.0741)	0.67 (±0.0368)
Lactate (media-CAS: 50-21-5; 20)	Malate shuttling towards lactate ($m_2/\Sigma m$)	55.1 (±6.42)	53.7 (±5.1)	55.5 (±1.3)
Lactate (media-CAS: 50-21-5; 22B)	Peak-area (abundance)	54,795 (±41,284)	23,286 (±6,449)	30,396 (±5,440)
Glutamate (media-CAS: 617-65-2; 76)	^{13}C-labeled fraction (C_2–C_5 fragment) (Σm)	1.37 (±0.0284)	2.18 (±0.768)	1.64 (±0.0817)*
Glutamate (media-CAS: 617-65-2; 77)	^{13}C content (C_2–C_5 fragment) (Σm_n)	0.02 (±0.0007)	0.06 (±0.0329)	0.03 (±0.002)*
Glutamate (media-CAS: 617-65-2; 79)	^{13}C-m_2 (m/z 200) ($m_2/\Sigma m$)	35.4 (±0.374)	28 (±6.87)	37.4 (±0.615)*
Glutamate (media-CAS: 617-65-2; 80)	^{13}C-m_3 (m/z 201) ($m_3/\Sigma m$)	2.51 (±0.616)	5.81 (±2.48)	3.31 (±0.792)
Glutamate (media-CAS: 617-65-2; 81)	^{13}C-m_4 (m/z 202) ($m_4/\Sigma m$)	9.37 (±0.387)	25.8 (±15.5)	10.7 (±0.792)
Glutamate (media-CAS: 617-65-2; 87B)	Peak-area (abundance)	159,534 (±18,546)	84,404 (±28,071)*	98,584 (±12,619)*
Stearic acid (pellet-CAS: 57-11-4; 107)	^{13}C-labeled fraction (m/z 298) (Σm)	52.6 (±2.18)	52.8 (±0.642)	49.8 (±0.904)[a]
Stearic acid (pellet-CAS: 57-11-4; 108)	^{13}C content (m/z 298) (Σm_n)	4.43 (±0.19)	4.43 (±0.0553)	4.18 (±0.0766)[a]
Stearic acid (pellet-CAS: 57-11-4; 114B)	Peak-area (abundance)	28,695 (±1,969)	25,010 (±3,332)	32,231 (±3,850)
RNA ribose (pellet-CAS: 50-69-1; 301)	^{13}C-labeled fraction (C_3-C_5) (Σm)	1.76 (±0.188)	2.85 (±0.38)	3.07 (±0.552)

(continued)

Table 15.1 (continued)

Metabolite (source-data-matrix-file-log)	Isotopomer fragment dimension	HepG2 (10 % DMSO)	HepG2 (1 μM Rosiglit)	HepG2 (10 μM Rosiglit)
RNA ribose (pellet-CAS: 50-69-1; 302)	^{13}C content (C_3–C_5) (Σm_n)	0.03 (±0.0051)	0.06 (±0.0091)*	0.06 (±0.0145)

&source-data-matrix-file-log: source of metabolite, i.e., culture media or pellets with raw data locator file number
$M_n/\Sigma m$: isotopomer/^{13}C-labeled fraction as SUM($m_1 + m_2 + \ldots + m_n$) is shown as percent of total ion current (TIC) instead of fraction of 1
Σm_n: molar enrichment (ME) ^{13}C content as SUM($1\times m_1 + 2\times m_2 + \ldots + n\times m_n$) (Lee et al. 1992)
Number of observations per group: $n = 3$ (±SD)
CAS chemical abstracts service registry number
*$P < 0.05$ vs. 10 % DMSO control
[a]$P < 0.05$ vs. 1 μM rosiglitazone (escalating rosiglitazone dosing comparison between 1 μM and 10 μM rosiglitazone in HepG2 cells, where cells have been cultured in the same type and tracer-containing media as described in Harrigan et al.)

^{13}C isotopomer associations) either from rosiglitazone dosing or its ^{13}C-stearic acid, cross-labeled from [1,2-$^{13}C_2$]-D-glucose, as the independent variable (explanatory variable). We observed partial high correlations between ^{13}C glucose tracer uptake and lactate's ^{13}C-labeling patterns, which mark the Warburg phenotype (Yang et al. 2013; Boros et al. 2013). On the other hand, there were strong associations among ^{13}C-glutamate, RNA ribose, and lactate labeling, when the effect of glucose uptake as a controlling random variable was replaced with that of the cross-labeled ^{13}C-stearate fraction from the glucose tracer.

Both studies showed an inhibition of lactate production in response to rosiglitazone treatment, which is consistent with decreasing the Warburg effect in tumor cells, one of rosiglitazone's known biological effects. While decreased lactate production is a reliable efficacy response, increased ^{13}C labeling from both tracers is more consistent with toxicity response demonstrating RNA synthesis/turnover-dependent peroxide scavenging by NADPH availability via increased pentose cycle flux. We believe that the isotopolome can be tied to clinical and preclinical outcomes and current surrogate biomarkers that will yield "new mechanistic" markers as measures of drug efficacy (Vamecq et al. 2012) and toxicity (Sonko et al. 2011). These new mechanistic tracer efficacy or toxicity markers could potentially be further qualified and defined for specific "concept (s) of use" during in vitro studies (Beger and Colatsky 2011).

In conclusion, there are significant improvements in associations between [1,2-$^{13}C_2$]-D-glucose tracer deriving intracellular stearate to lactate, glutamate, and ribose ^{13}C labeling (Fig. 15.6) and with that obtained with an extracellular stearic acid tracer in response to rosiglitazone treatment with the central mechanism of increasing fatty acid beta-oxidation and turnover.

Table 15.2 Targeted ^{13}C isotopolome (^{13}C-labeled metabolome) matrix of rosiglitazone-treated HepG2 (primary hepatocellular carcinoma) cells using [1,2-$^{13}C_2$]-D-glucose as the single tracer and GC-MS in 72 h cultures

Metabolite (source-data-matrix-file-log)	Isotopomer fragment dimension	HepG2 (10 % DMSO)	HepG2 (1 μM Rosiglit)	HepG2 (10 μM Rosiglit)
Lactate (media-CAS: 50-21-5; 17)	^{13}C-labeled fraction (Σm)	21.5 (±0.629)	22.8 (±0.687)	23.6 (±0.0471)
Lactate (media-CAS: 50-21-5; 20)	Malate shuttling towards lactate ($m_2/\Sigma m$)	70.9 (±0.0925)	69.2 (±0.548)	70.5 (±0.682)
Lactate (media-CAS: 50-21-5; 22B)	Peak-area (abundance)	148,615 (±116,074)	35,950 (±7,661)	35,674 (±12,175)
Glutamate (media-CAS: 617-65-2; 76)	^{13}C-labeled fraction (C_2–C_5 fragment) (Σm)	17 (±0.231)	18.8 (±0.408)*	19.2 (±0.59)*
Glutamate (media-CAS: 617-65-2; 77)	^{13}C content (C_2–C_5 fragment) (Σm_n)	0.29 (±0.004)	0.33 (±0.0062)*	0.34 (±0.0098)*
Glutamate (media-CAS: 617-65-2; 79)	^{13}C-m_2 (m/z 200) ($m_2/\Sigma m$)	49.8 (±0.184)	49.7 (±0.336)	50.5 (±0.412)
Glutamate (media-CAS: 617-65-2; 80)	^{13}C-m_3 (m/z 201) ($m_3/\Sigma m$)	8.18 (±0.0171)	8.32 (±0.0682)	8.3 (±0.0323)*
Glutamate (media-CAS: 617-65-2; 81)	^{13}C-m_4 (m/z 202) ($m_4/\Sigma m$)	2.45 (±0.0581)	2.88 (±0.0158)*	3 (±0.0214)*,a
Glutamate (media-CAS: 617-65-2; 87B)	Peak-area (abundance)	33,445 (±4,507)	42,381 (±28,935)	47,175 (±3,164)
Stearic acid (pellet-CAS: 57-11-4; 107)	^{13}C-labeled fraction (m/z 298) (Σm)	12.9 (±2.33)	18.1 (±4.04)	22.4 (±2.33)*
Stearic acid (pellet-CAS: 57-11-4; 108)	^{13}C content (m/z 298) (Σm_n)	0.36 (±0.0681)	0.51 (±0.119)	0.64 (±0.0679)*
Stearic acid (pellet-CAS: 57-11-4; 114B)	Peak-area (abundance)	448,116 (±184,694)	369,434 (±155,377)	170,589 (±24,930)
RNA ribose (pellet-CAS: 50-69-1; 301)	^{13}C-labeled fraction (C_3–C_5) (Σm)	33.9 (±1.75)	36.4 (±0.231)	37.4 (±0.596)

(continued)

Table 15.2 (continued)

Metabolite (source-data-matrix-file-log)	Isotopomer fragment dimension	HepG2 (10 % DMSO)	HepG2 (1 μM Rosiglit)	HepG2 (10 μM Rosiglit)
RNA ribose (pellet-CAS: 50-69-1; 302)	^{13}C content (C_3–C_5) (Σm_n)	0.58 (±0.0294)	0.61 (±0.0043)	0.63 (±0.0101)

Controls are HepG2 cells treated with 10 % DMSO. $N = 3$, average (±SD)
&source-data-matrix-file-log: source of metabolite, i.e., culture media or pellets with raw data locator file number
$M_n/\Sigma m$: isotopomer/^{13}C-labeled fraction as SUM($m_1 + m_2 + \cdots + m_n$) is shown as percent of total ion current (TIC) instead of fraction of 1
Σm_n: molar enrichment (ME) ^{13}C content as SUM($1 \times m_1 + 2 \times m_2 + \cdots + n \times m_n$) (Lee et al. 1992)
Number of observations per group: $n = 3$ (±SD)
CAS chemical abstracts service registry number
*$P < 0.05$ vs. 10 % DMSO control
[a]$P < 0.05$ vs. 1 μM rosiglitazone (escalating rosiglitazone dosing comparison between 1 μM and 10 μM rosiglitazone in HepG2 cells, where cells have been cultured in the same type and tracer-containing media as described in Harrigan et al.)

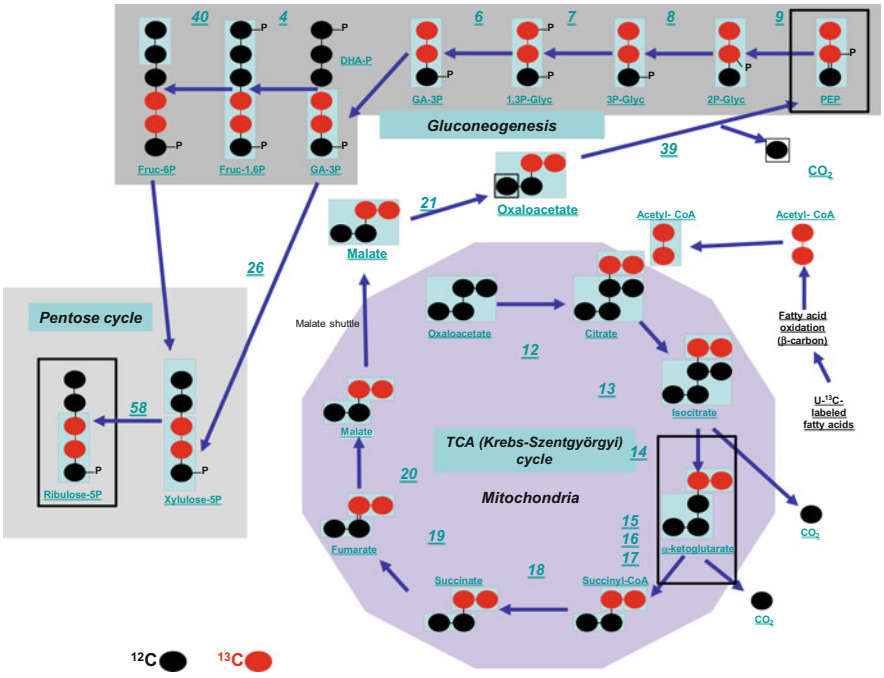

Fig. 15.3 Overview of RNA ribose, lactate, and glutamate labeling from [U-$^{13}C_{18}$]-stearate deriving acetyl-CoA and beta-carbon oxidation. For identifying enzymes and metabolite, please see Tables 15.3 and 15.4, respectively

Table 15.3 Enzyme identifiers by Arabic numbers that refer to article panels (Fig. 15.3)

001	Glucokinase	EC 2.7.1.1	en.wikipedia.org/wiki/Glucokinase
002	Glucose-6-phosphate isomerase	EC 5.3.1.9	en.wikipedia.org/wiki/Glucose_phosphate_isomerase
003	Phosphofructokinase 1	EC 2.7.1.11	en.wikipedia.org/wiki/Phosphofructokinase_1
004	Aldolase A	EC 4.1.2.13	en.wikipedia.org/wiki/Aldolase_A
005	Triosephosphate isomerase	EC 5.3.1.1	en.wikipedia.org/wiki/Triosephosphateisomerase
006	Glyceraldehyde-3-phosphate dehydrogenase	EC 1.2.1.12	en.wikipedia.org/wiki/Glyceraldehyde_3-phosphate_dehydrogenase
007	Phosphoglycerate kinase	EC 2.7.2.3	en.wikipedia.org/wiki/Phosphoglycerate_kinase
008	Phosphoglycerate mutase	EC 5.4.2.1	en.wikipedia.org/wiki/Phosphoglycerate_mutase
009	Enolase	EC 4.2.1.11	en.wikipedia.org/wiki/Enolase
010	Pyruvate kinase	EC 2.7.1.40	en.wikipedia.org/wiki/Pyruvate_kinase
011	Pyruvate dehydrogenase	EC 1.2.4.1	en.wikipedia.org/wiki/Pyruvate_dehydrogenase
012	Citrate synthase	EC 2.3.3.1	en.wikipedia.org/wiki/Citrate_synthase
013	Aconitase	EC 4.2.1.3	en.wikipedia.org/wiki/Aconitase
014	Isocitrate dehydrogenase	EC 1.1.1.42	en.wikipedia.org/wiki/Isocitrate_dehydrogenase
015	Oxoglutarate dehydrogenase	EC 1.2.4.2	en.wikipedia.org/wiki/Isocitrate_dehydrogenase
016	Dihydrolipoyl succinyltransferase	EC 2.3.1.61	en.wikipedia.org/wiki/Alpha-ketoglutarate_dehydrogenase
017	Dihydrolipoyl dehydrogenase	EC 1.8.1.4	en.wikipedia.org/wiki/Alpha-ketoglutarate_dehydrogenase
018	Succinyl coenzyme A synthetase	EC 6.2.1.5	en.wikipedia.org/wiki/Succinyl_coenzyme_A_synthetase
019	Succinate dehydrogenase	EC 1.3.5.1	en.wikipedia.org/wiki/Succinate_dehydrogenase
020	Fumarate hydratase	EC 4.2.1.2	en.wikipedia.org/wiki/Fumarase
021	Malate dehydrogenase	EC 1.1.1.37	en.wikipedia.org/wiki/Malate_dehydrogenase
022	Glucose-6-phosphate dehydrogenase	EC 1.1.1.49	en.wikipedia.org/wiki/Glucose-6-phosphate_dehydrogenase
023	Phosphogluconate 2-dehydrogenase	EC 1.1.1.43	en.wikipedia.org/wiki/Phosphogluconate_2-dehydrogenase

(continued)

Table 15.3 (continued)

024	Ribose-5-phosphate isomerase	EC 5.3.1.6	en.wikipedia.org/wiki/Ribose-5-phosphate_isomerase
025	Ribose-phosphate diphosphokinase: phosphoribosyl pyrophosphate synthetase	EC 2.7.6.1	en.wikipedia.org/wiki/Ribose-phosphate_diphosphokinase
026	Transketolase	EC 2.2.1.1	en.wikipedia.org/wiki/Transketolase
027	Transaldolase	EC 2.2.1.2	en.wikipedia.org/wiki/Transaldolase
028	Glucose-6-phosphatase: Glc-6-Pase	EC 3.1.3.9	en.wikipedia.org/wiki/Glucose_6-phosphatase
031	Lactate dehydrogenase	EC 1.1.1.27	en.wikipedia.org/wiki/Lactate_dehydrogenase
032	Pyruvate carboxylase	EC 6.4.1.1	en.wikipedia.org/wiki/Pyruvate_carboxylase
033	Fatty acid synthase	EC 2.3.1.85	en.wikipedia.org/wiki/Fatty_acid_synthase
034	Acyl-CoA dehydrogenase	EC 1.3.99.3	en.wikipedia.org/wiki/Acyl_CoA_dehydrogenase
035	Enoyl-CoA hydratase	EC 4.2.1.17	en.wikipedia.org/wiki/Enoyl_CoA_hydratase
036	L-β-Hydroxyacyl-CoA dehydrogenase	EC 1.1.1.35	en.wikipedia.org/wiki/Beta_oxidation
037	Acetyl-CoA C-acyltransferase	EC 2.3.1.16	en.wikipedia.org/wiki/%CE%92-ketothiolase
039	Phosphoenolpyruvate carboxykinase	EC 4.1.1.32	en.wikipedia.org/wiki/Phosphoenolpyruvate_carboxykinase
040	Fructose 1,6-bisphosphatase	EC 3.1.3.11	en.wikipedia.org/wiki/Fructose_1,6-bisphosphatase
041	Beta-ketoacyl-ACP synthase	EC 2.3.1.41	en.wikipedia.org/wiki/Beta-ketoacyl-ACP_synthase
042	Beta-ketoacyl-ACP reductase	EC 1.1.1.100	en.wikipedia.org/wiki/%CE%92-Ketoacyl_ACP_reductase
043	3-Hydroxyacyl ACP	EC 4.2.1.134	en.wikipedia.org/wiki/3-Hydroxyacyl_ACP_dehydratase
044	Enoyl-acyl carrier protein reductase	EC 1.3.1.9	en.wikipedia.org/wiki/Enoyl_ACP_reductase
045	Acetyl-coenzyme A acetyltransferase	EC 2.3.1.9	en.wikipedia.org/wiki/Acetyl-Coenzyme_A_acetyltransferase
046	HMG-CoA synthase	EC 2.3.3.10	en.wikipedia.org/wiki/HMG-CoA_synthase
047	HMG-CoA reductase	EC 1.1.1.34	en.wikipedia.org/wiki/HMG-CoA_reductase
048	Mevalonate kinase	EC 2.7.1.36	en.wikipedia.org/wiki/Mevalonate_kinase

(continued)

Table 15.3 (continued)

049	Phosphomevalonate kinase	EC 2.7.4.2	en.wikipedia.org/wiki/Phosphomevalonate_kinase
050	Pyrophosphomevalonate decarboxylase	EC 4.1.1.33	en.wikipedia.org/wiki/Pyrophosphomevalonate_decarboxylase
051	Isopentenyl-diphosphate delta-isomerase	EC 5.3.3.2	en.wikipedia.org/wiki/Isopentenyl-diphosphate_delta_isomerase
052	Phosphoglucomutase	EC 5.4.2.2	en.wikipedia.org/wiki/Phosphoglucomutase
053	Glycogen synthase	EC 2.4.1.11	en.wikipedia.org/wiki/Glycogen_synthase
054	Glutamate dehydrogenase	EC 1.4.1.3	en.wikipedia.org/wiki/Glutamate_dehydrogenase
055	ATP citrate lyase	EC 2.3.3.8	en.wikipedia.org/wiki/ATP_citrate_lyase
056	Acetyl-CoA carboxylase	EC 6.4.1.2	en.wikipedia.org/wiki/Acetyl-CoA_carboxylase
057	Glycogen phosphorylase	EC 2.4.1.1	en.wikipedia.org/wiki/Glycogen_phosphorylase
058	Ribulose-phosphate 3-epimerase	EC 5.1.3.1	en.wikipedia.org/wiki/Ribulose-phosphate_3-epimerase
059	Xylulokinase	EC 2.7.1.17	en.wikipedia.org/wiki/Xylulokinase
060	D-Xylose aldose-ketose-isomerase	EC 5.3.1.5	en.wikipedia.org/wiki/Xylose_isomerase
061	Dimethylallyltranstransferase	EC 2.5.1.1	en.wikipedia.org/wiki/Farnesyl_pyrophosphate_synthase
062	Farnesyl-diphosphate farnesyltransferase	EC 2.5.1.21	en.wikipedia.org/wiki/Squalene_synthase
063	Squalene monooxygenase	EC 1.14.99.7	en.wikipedia.org/wiki/Squalene_monooxygenase
064	2,3-Oxidosqualene-(cycloartenol) cyclase	EC 5.4.99.7	en.wikipedia.org/wiki/Cycloartenol_synthase
065	Sterol-carrier protein		en.wikipedia.org/wiki/Sterol_carrier_protein
066	DOXP synthase	EC 2.2.1.7	en.wikipedia.org/wiki/DOXP_synthase
067	DXP reductoisomerase	EC 1.1.1.267	en.wikipedia.org/wiki/DOXP_reductase
068	2-C-Methyl-D-erythritol 2,4-cyclodiphosphate synthase	EC 4.6.1.12	en.wikipedia.org/wiki/4-diphosphocytidyl-2-C-methyl-D-erythritol_synthase
069	4-(Cytidine 5'-diphospho)-2-C-methyl-D-erythritol kinase	EC 2.7.1.148	en.wikipedia.org/wiki/4-diphosphocytidyl-2-C-methyl-D-erythritol_kinase

(continued)

Table 15.3 (continued)

070	2-C-Methyl-D-erythritol 2,4-cyclodiphosphate synthase	EC 4.6.1.12	en.wikipedia.org/wiki/2-C-methyl-D-erythritol_2,4-cyclodiphosphate_synthase
071	4-Hydroxy-3-methylbut-2-en-1-yl diphosphate synthase	EC 1.17.4.3	en.wikipedia.org/wiki/HMB-PP_synthase
072	4-Hydroxy-3-methylbut-2-enyl diphosphate reductase	EC 1.17.1.2	en.wikipedia.org/wiki/HMB-PP_reductase
073	Palmitoyl-(protein) hydrolase	EC 3.1.2.22	en.wikipedia.org/wiki/Palmitoyl%28protein%29_hydrolase
074	Acyl-CoA:acetyl-CoA C-acyltransferase	EC 2.3.1.16	en.wikipedia.org/wiki/Acetyl-CoA_C-acyltransferase
075	Long-chain-(S)-3-hydroxyacyl-CoA: NAD + oxidoreductase	EC 1.1.1.211	en.wikipedia.org/wiki/3-hydroxyacyl-CoA_dehydrogenase
076	Long-chain-(3S)-3-hydroxyacyl-CoA hydro-lyase	EC 4.2.1.74	en.wikipedia.org/wiki/Long-chain-enoyl-CoA_hydratase
077	Acyl-CoA:NADP + 2-oxidoreductase	EC 1.3.1.8	en.wikipedia.org/wiki/Acyl-CoA_dehydrogenase_%28NADP%2B%29
078	Stearoyl-CoA 9-desaturase	EC 1.14.19.1	en.wikipedia.org/wiki/Stearoyl-CoA_9-desaturase

While fatty acid oxidation can readily be measured using mass isotopomer distribution analysis (MIDA) in ^{13}C-labeled CO_2 and numerous TCA and pentose cycle ribose products in HepG2 cells with [U-$^{13}C_{18}$]-stearic acid (Fig. 15.7a), the Warburg effect, glycolysis, and pentose cycling are most efficiently determined with ^{13}C-glucose in a wide range of in vitro cell systems under various growth conditions (Fig. 15.7b).

Alternatively, targeted [1,2-$^{13}C_2$]-D-glucose fate associations, as the single metabolic tracer method in the same cell system, can reveal cross ^{13}C-labeled stearate breakdown and the Warburg effect, glycolysis, as well as TCA and pentose cycle metabolism as the single tracer substrate in the metabolome of tumor cells (Fig. 15.8).

Therefore, we recommend reevaluation of drug efficacy and mechanism of action studies for contemporary metabolomics investigations using multiple parallel or mixed tracer approaches. Herein, we recommend the use of a single glucose tracer and targeting its fate via cross-labeled multiple substrate-product patterns as independent explanatory variables for determining efficacy and phenotype-related associations in single experiments. The single glucose tracer approach, which inherently corrects for ^{13}C-labeled fractions and positional ^{13}C labeling in all targeted products as an internal standard throughout the ^{13}C-labeled metabolome (isobolome), minimizes the unforeseen complications of altered extra- and intracellular metabolome cross talk during efficacy testing.

Table 15.4 Metabolite identifiers in alphabetic order that refer to article panels (Fig. 15.3)

(α)Ketoglutarate	Alpha-ketoglutarate	en.wikipedia.org/wiki/Alpha-ketoglutaric_acid
1,3P-Glyc	Glycerol-1,3-bisphosphate	en.wikipedia.org/wiki/Glycerol
2,3-O-Squalene	2,3-Oxidosqualene	en.wikipedia.org/wiki/Squalene_oxide
2P-Glyc	Glycerol 2-phosphate	en.wikipedia.org/wiki/Glycerol
3P-Glyc	Glycerol 3-phosphate	en.wikipedia.org/wiki/Glycerol_3-phosphate
6-Phosphogluc	6-Phosphogluconate	en.wikipedia.org/wiki/6-Phosphogluconate
Acetoacetyl-CoA	Acetoacetyl-CoA	en.wikipedia.org/wiki/Acetoacetyl-CoA
Acetyl-CoA	Acetyl-CoA	en.wikipedia.org/wiki/Acetyl-CoA
ATP	Adenosine triphosphate	en.wikipedia.org/wiki/Adenosine_triphosphate
CMP	Cytidine monophosphate	en.wikipedia.org/wiki/Cytidine_monophosphate
CDP-ME	4-Diphosphocytidyl-2-C-methylerythritol	en.wikipedia.org/wiki/4-diphosphocytidyl-2-C-methylerythritol
CDP-MEP	4-Diphosphocytidyl-2-C-methyl-D-erythritol 2-phosphate	en.wikipedia.org/wiki/4-diphosphocytidyl-2-C-methyl-D-erythritol_2-phosphate
Chol	Cholesterol	en.wikipedia.org/wiki/Cholesterol
Cit	Citrate	en.wikipedia.org/wiki/Citrate
CO_2	Carbon dioxide	en.wikipedia.org/wiki/Carbon_dioxide
CTP	Cytidine triphosphate	en.wikipedia.org/wiki/Cytidine_triphosphate
DA-5-PP	Dimethylallyl-5-pyrophosphate	en.wikipedia.org/wiki/Dimethylallyl_pyrophosphate
DOXP	1-Deoxy-D-xylulose 5 phosphate	en.wikipedia.org/wiki/1-Deoxy-D-xylulose_5-phosphate
DHA-P	Dihydroxyacetone-phosphate	en.wikipedia.org/wiki/Dihydroxyacetone
Farnesyl-PP	Farnesyl pyrophosphate	en.wikipedia.org/wiki/Farnesyl_pyrophosphate
Fruc-1,6P	Fructose-1,6-bisphosphate	en.wikipedia.org/wiki/Fructose
Fruc-6P	Fructose-6-phosphate	en.wikipedia.org/wiki/Fructose_6-phosphate
Fum	Fumarate	en.wikipedia.org/wiki/Fumaric_acid
GA-3P	Glyceraldehyde 3-phosphate	en.wikipedia.org/wiki/Glyceraldehyde_3-phosphate
Geranyl-PP	Geranyl pyrophosphate	en.wikipedia.org/wiki/Geranyl_pyrophosphate
Gluc	Glucose (dextrose)	en.wikipedia.org/wiki/Glucose
Gluc-1P	Glucose-1-phosphate	en.wikipedia.org/wiki/Glucose_1-phosphate
Gluc-6P	Glucose-6-phosphate	en.wikipedia.org/wiki/Glucose-6-phosphate
Glutam	Glutamate	en.wikipedia.org/wiki/Glutamate
Gly	Glycogen	en.wikipedia.org/wiki/Glycogen

(continued)

Table 15.4 (continued)

(α)Ketoglutarate	Alpha-ketoglutarate	en.wikipedia.org/wiki/Alpha-ketoglutaric_acid
HMB-PP	(E)-4-Hydroxy-3-methylbut-2-enyl pyrophosphate	en.wikipedia.org/wiki/%28E%29-4-Hydroxy-3-methyl-but-2-enyl_pyrophosphate
HMG-CoA	3-Hydroxy-3-methylglutaryl-coenzyme A	en.wikipedia.org/wiki/HMG-CoA
Isocit	Isocitrate	en.wikipedia.org/wiki/Isocitric_acid
Isopent-5-PP	Isopentenyl-5-pyrophosphate	en.wikipedia.org/wiki/Isopentenyl_pyrophosphate
Lact	Lactic acid	en.wikipedia.org/wiki/Lactic_acid
Lanost	Lanosterol	en.wikipedia.org/wiki/Lanosterol
Malate	Malic acid	en.wikipedia.org/wiki/Malate
Malonyl-CoA	Malonyl-CoA	en.wikipedia.org/wiki/Malonyl-CoA
MEP	2-C-Methylerythritol 4-phosphate	en.wikipedia.org/wiki/2-C-methylerythritol_4-phosphate
MEcPP	2-C-Methyl-D-erythritol-2,4-cyclopyrophosphate	en.wikipedia.org/wiki/2-C-methyl-D-erythritol_2,4-cyclopyrophosphate
Meval acid	Mevalonic acid	en.wikipedia.org/wiki/Mevalonic_acid
Meval-5-P	Phosphomevalonic acid	en.wikipedia.org/wiki/Phosphomevalonic_acid
Meval-5-PP	Mevalonate-5-pyrophosphate	en.wikipedia.org/wiki/Phosphomevalonic_acid
NADH	Nicotinamide adenine dinucleotide	en.wikipedia.org/wiki/NADH
NADPH	Nicotinamide adenine dinucleotide phosphate	en.wikipedia.org/wiki/NADPH
Oleate	Oleic acid	en.wikipedia.org/wiki/Oleic_acid
OAA	Oxaloacetic acid	en.wikipedia.org/wiki/Oxaloacetic_acid
Palmitate	Palmitatic acid	en.wikipedia.org/wiki/Palmitate
PEP	Phosphoenolpyruvate	en.wikipedia.org/wiki/Phosphoenolpyruvate
Pyruvate	Pyruvic acid	en.wikipedia.org/wiki/Pyruvic_acid
Ribose-5P	Ribose 5-phosphate	en.wikipedia.org/wiki/Ribose_5-phosphate
R-ulose-5P	Ribulose 5-phosphate	en.wikipedia.org/wiki/Ribulose_5-phosphate
Stearate	Stearic acid	en.wikipedia.org/wiki/Stearic_acid
Squal	Squalene	en.wikipedia.org/wiki/Squalene
Succin	Succinate	en.wikipedia.org/wiki/Succinate
Succinyl-CoA	Succinyl-CoA	en.wikipedia.org/wiki/Succinyl-CoA
UDP	Uridine diphosphate	en.wikipedia.org/wiki/Uridine_diphosphate
UDP-gluc	UDP-glucose	en.wikipedia.org/wiki/UDP-glucose
Xyl	Xylose	en.wikipedia.org/wiki/Xylose
Xylul	Xylulose	en.wikipedia.org/wiki/Xylulose
Xylulose-5P	Xylulose-5P	en.wikipedia.org/wiki/Xylulose-5-phosphate

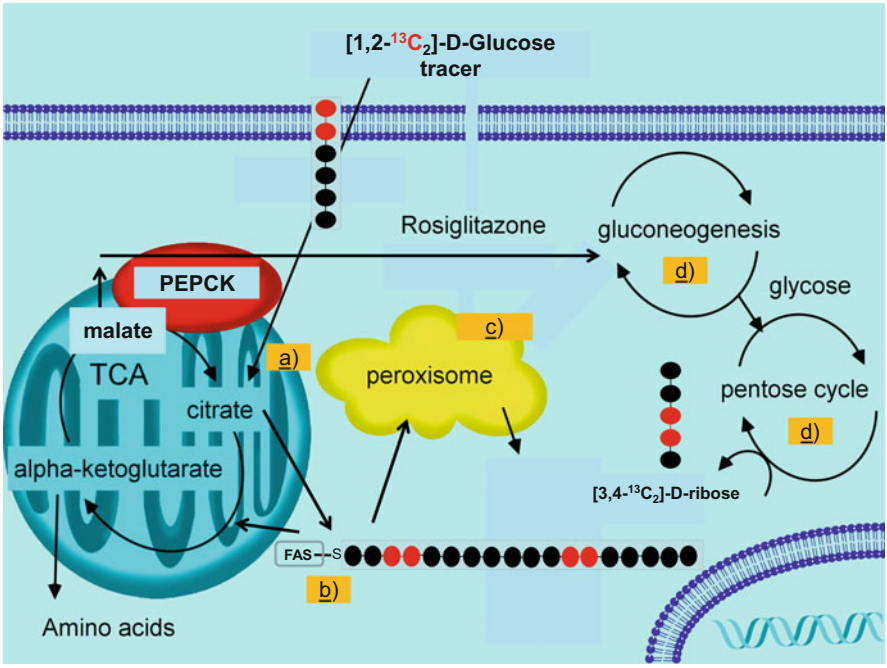

Fig. 15.4 Extracellular [1,2-$^{13}C_2$]-D-glucose tracer substrate entry and its metabolic hubs after rosiglitazone action in HepG2 cells. (**a**) Rosiglitazone increases lipogenic citrate labeling from [1,2-$^{13}C_2$]-D-glucose after increasing long-chain fatty acid degradation while routing, (**b**) newly labeled malonyl-CoA flux towards stearic acid synthesis/turnover, followed by (**c**) peroxisomal remodeling and intracellular fatty acid mobilization towards, (**d**) [3,4-$^{13}C_2$]-D-pentose and hexose labeling. Please note that acetyl-CoA can also yield [4,5-$^{13}C_2$]-D-pentose, based on labeled oxaloacetate recycling in the cycle

15.1 Materials and Methods

Two non-radiating stable isotope tracer carbon-labeled substrates were used in this metabolic flux analysis study: ***a)*** [1,2-$^{13}C_2$]-D-Glucose was purchased with >99 % purity and 99 % isotope enrichment for each position from Cambridge Isotope Laboratories, Inc. (Andover, MA, USA), and ***b)*** [U-$^{13}C_{18}$]-stearic acid (Spectra Stable Isotopes, Spectra Gases Inc., Branchburg, NJ). Rosiglitazone was provided by Pfizer, Inc., under a material transfer agreement.

15.1.1 Cells and Cell Culture

Human liver hepatocellular (epithelial) carcinoma HepG2 cells were purchased from American Type Culture Collection (ATCC, Manassas, VA, USA). HepG2

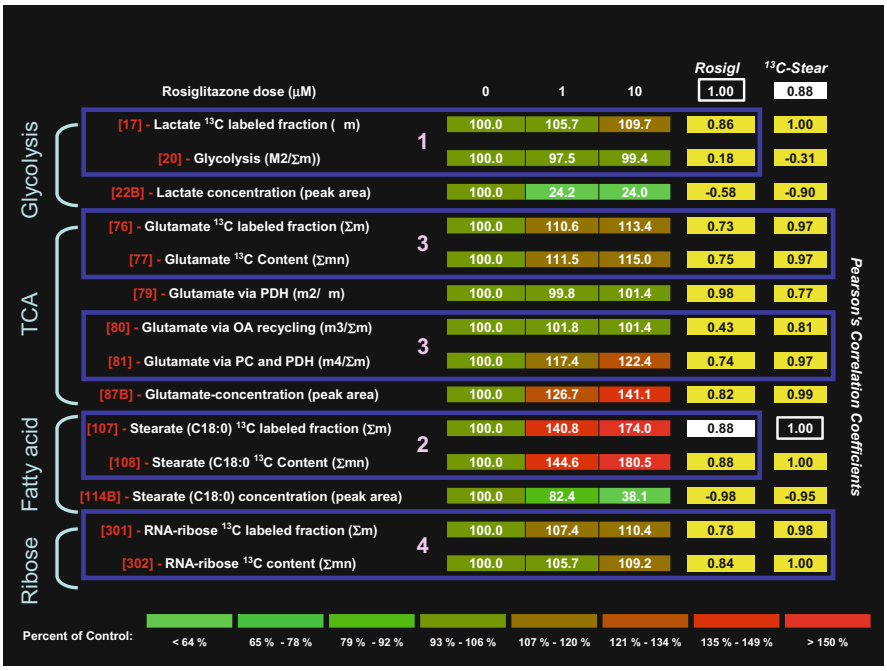

Fig. 15.5 EZTopolome (EZTop[1,2-$^{13}C_2$]-D-glucose) of in vitro grown HepG2 liver cells, which serves as the color-assisted visual isotopolome-wide matrix screening tool. There is maintained lactate labeling (shown in *blue box* 1—line 17 and glucose oxidation—please also see reference[1] SiDMAParray for glucose uptake/oxidation data with rosiglitazone dosing), with expected high and unaltered glycolysis (line 20). Importantly, the EZTop shows increased stearate labeling (shown in *blue box* 2—line 107, line 108) from glucose, which is responsive to rosiglitazone treatment, shown by the relatively high (0.88) positive correlation coefficient between rosiglitazone dosing and intracellular stearate ^{13}C-labeled fractions (and ^{13}C content). Glutamate's ^{13}C meta-labeling from the glucose tracer shows much improved correlation coefficients with that of cross-labeled stearate fractions as the independent explanatory variable (shown in *blue box* 3—lines 76, 77, 80, 81). Rosiglitazone, as expected, increases glucose-derived cross-labeled ^{13}C-stearate carbon labeling in RNA-derived ribose (shown in *blue box* 4—line 301, line 302), where correlation coefficients are close to one with cross-labeled stearate as the reference range. The [1,2-$^{13}C_2$]-D-glucose *EZ*Topolome returns correlation coefficients between rosiglitazone dosing (*Rosigl* column, *yellow*) or cross-^{13}C-labeled stearate (*^{13}C-Stear* column, *yellow*) as reference variables (*white boxes* = 1) and the rest of the [1,2-$^{13}C_2$]-D-glucose isotopolome

cells have an average doubling time of 34 h in DMEM with 10 % fetal bovine serum and 2.5 % horse serum (Gibco/BRL, Gaithersburg, MD) in the presence of antibiotics. The cells were incubated at 37 °C, 5 % CO_2, and 95 % humidity and passed by using trypsin 0.25 % (Gibco/BRL) no more than three times after receipt from the ATCC and prior to use in this study. HepG2 cells have previously been used in both in vitro and in vivo experiments and responded to treatment with troglitazone and other compounds with characteristic metabolic profile changes showing altered macromolecule synthesis and fatty acid cycling (Lee et al. 1997). Tracer-labeled

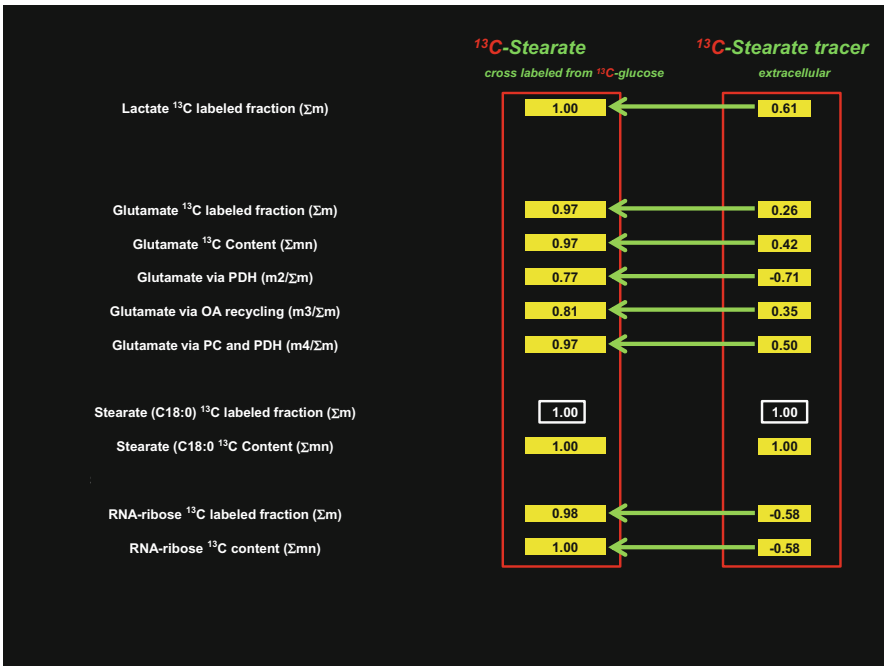

Fig. 15.6 Improvements in correlations between intracellular ^{13}C-labeled stearic acid fractions as the explanatory variable (shown in *white squares* with default correlation coefficient = 1), cross-labeled from the [1,2-$^{13}C_2$]-D-glucose tracer (column labeled as such in the *left red square*), in comparison with extracellular [U-$^{13}C_{18}$]-stearic acid (column labeled as such in the *right red square*) as the metabolic tracer. Correlation coefficients show the dependence (dependent or response variables) of selected multiple product isotopomers. We observed much improved correlations (shown by *green arrows*), i.e., closer associations with rosiglitazone's efficacy markers, reflecting this drug's central mechanism of stearate degrading action, from ^{13}C glucose-derived stearate in comparison with that of the extracellular stearate tracer

parallel cultures of HepG2 cells were used in this study as controls to compare vehicle (DMSO)-treated cell cultures to rosiglitazone treatment in an escalating regime of drug treatment.

Seventy-five percent confluent cultures of HepG2 cells were incubated in either [1,2-$^{13}C_2$]-D-glucose or [U-$^{13}C_{18}$]-stearate-containing media (100 mg/dl total glucose concentration = 5 mM; 50 % isotope enrichment; or 0.5 mM uniformly labeled stearate). Cells were plated at a density of 10^6 per T75 culture flask, and rosiglitazone was added in two concentrations, 1 μM or 10 μM dissolved in 10 % DMSO and 90 % culture media. Control cultures were treated with vehicle (10 % DMSO) only. The doses of rosiglitazone for the present study were selected based on in vitro experiments demonstrating that these drugs effectively control glucose levels via PPARγ activation in various human cell culture systems in the 1 μM to a 10 μM dose range [for review, see Otto et al. (2002)]. Drug treatments were carried out for 72 h in the presence of each tracer. Glucose and U-stearate ^{13}C tracer levels

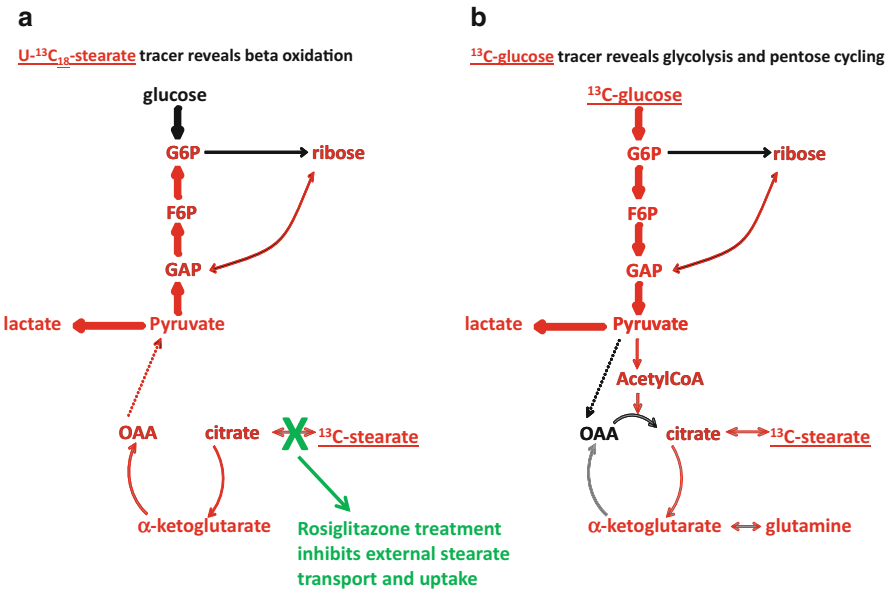

Fig. 15.7 Multiple ^{13}C-tracer substrates are used in metabolic profiling studies to reveal diverse metabolic phenotypes of tumor cells, where (**a**) uniformly ^{13}C-labeled stearic acid is used to study beta-oxidation and gluconeogenesis, ketogenic citrate labeling, and its recycling in the cytosol towards ribose labeling (*red arrows*) via mitochondria, while (**b**) ^{13}C-glucose is used to reveal the Warburg effect, glycolysis, pentose cycling and de novo (new) fatty acid synthesis in the cytoplasm. The *green cross* and *arrow* show limited stearate uptake after thiazolidinedione treatment, which is a limiting factor in multiple tracer studies by drug- and dose-related changes in tracer uptake (*G6P* glucose-6-phosphate, *F6P* fructose-6-phosphate, *GAP* glyceraldehyde-3-phosphate, *OAA* oxaloacetate)

in the medium were monitored using a Cobas Mira chemistry analyzer (Roche Diagnostics, Pleasanton, CA, USA). Fresh, tracer-enriched culture medium and drug treatments were applied every 24 h, three times during the experiment, in order to provide for the cells with steady tracer-enriched medium and drug doses throughout the 72 h experimental period. After 72 h the cells were scraped, spun, and frozen at −80 °C until further processing as described below.

15.2 RNA Ribose Stable Isotope Studies

For mass isotopomer analysis RNA ribose was isolated by acid hydrolysis of cellular RNA after Trizol (Invitrogen Life Technologies, Carlsbad, CA, USA) extraction from the cell pellets. Ribose was derivatized to its aldonitrile acetate form using hydroxylamine in pyridine with acetic anhydride (Supelco, Bellefonte,

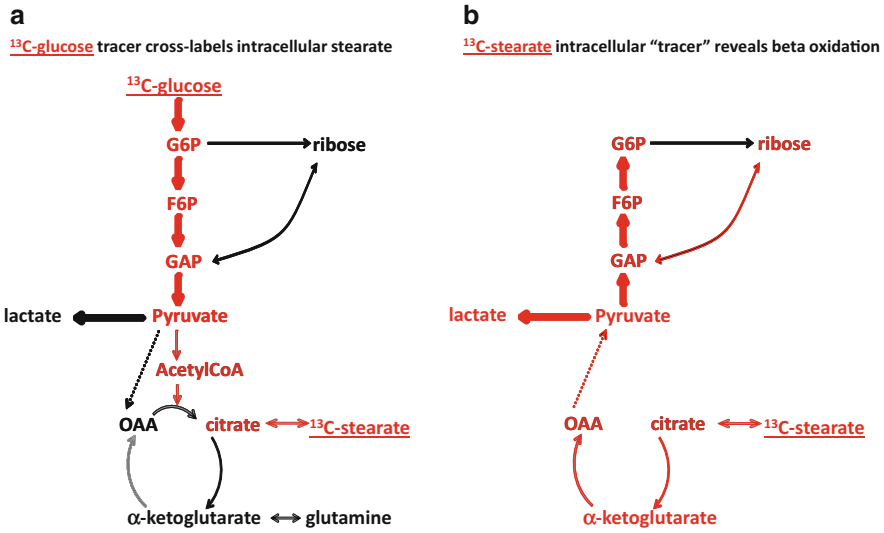

Fig. 15.8 Single [1,2-$^{13}C_2$]-D-glucose fate association study reveals diverse metabolic phenotypes of cultured tumor cells, where (**a**) [1,2-$^{13}C_2$]-D-glucose associations are used to reveal the Warburg effect, glycolysis, and pentose cycling in the cytoplasm, while (**b**) ^{13}C-stearate associations, cross-labeled from the glucose tracer, are used to study fatty acid oxidation and back labeling of products on specific carbon positions, lipogenic citrate synthesis, and its shuttling towards ketoglutarate(α) (*red arrows*) in mitochondria. Please note that cross-labeled stearate also labels lactate via gluconeogenesis and RNA ribose via the non-oxidative branch of the pentose cycle. There is no thiazolidinedione-related limiting action on internal stearate labeling from glucose (*G6P* glucose-6-phosphate, *F6P* fructose-6-phosphate, *GAP* glyceraldehyde-3-phosphate, *OAA* oxaloacetate)

PA, USA) before mass spectral analyses. We monitored the ion cluster around the *m*/*z* 256 (carbons 1–5 of ribose) (chemical ionization, CI) and *m*/*z* 217 (carbons 3–5 of ribose) and *m*/*z* 242 (carbons 1–4 of ribose) (electron impact ionization, EI) to determine molar enrichment and the positional distribution of ^{13}C in ribose. By convention, the base mass of ^{12}C compounds (with their derivatization agents) is given as m_0 as measured by mass spectrometry as described elsewhere (Katz et al. 1993). Ribose molecules labeled with a single ^{13}C atom on the first carbon position (m_1) recovered from RNA were used to gauge the ribose fraction produced by direct oxidation of glucose through the G6PD pathway. Ribose molecules labeled with ^{13}C on the first two carbon positions (m_2) were used to measure the fraction produced by transketolase. Doubly labeled ribose molecules (m_2 and m_4) on the fourth and fifth carbon positions were used to measure molar fraction produced by triosephosphate isomerase and transketolase (Boros et al. 2002). Because transketolase has the highest metabolic control coefficient in the non-oxidative branch of the pentose cycle (Sabate et al. 1995), we use the term *transketolase* throughout the paper. It should be noted, though, that transketolase and transaldolase, besides other enzymes, all are participants in non-oxidative pentose cycle metabolism in human cells.

15.2.1 Lactate

Lactate from the cell culture media (0.2 ml) was extracted by ethylene chloride after acidification with HCl. Lactate was derivatized to its propylamine-heptafluorobutyrate ester form, and the *m/z* 328 (carbons 1–3 of lactate) (chemical ionization, CI) was monitored for the detection of m_1 (recycled lactate through the PC) and m_2 (lactate produced by the Embden-Meyerhof-Parnas pathway) for the estimation of pentose cycle activity (Lee et al. 1998b). In this study we recorded the m_1/m_2 ratios in lactate produced and released by HepG2 cells in order to determine pentose cycle activity and pentose cycling versus anaerobic glycolysis in response to 1 μM and 10 μM rosiglitazone treatments.

15.2.2 Glutamate

^{13}C-label distribution in glutamate (glutamic acid), which is synthesized from α-ketoglutaric acid of the TCA cycle, from tracer-labeled glucose or stearate is suitable for determining mitochondrial glucose and fatty acid disposal via anabolic substrate use within the cycle, also known as anaplerotic flux. For glutamate extraction tissue culture medium (1 ml) was first treated with 1 ml of 6 % perchloric acid, and the supernatant was passed through a 3 cm^3 Dowex-50 (H+) column. Amino acids were eluted with 15 ml 2 N ammonium hydroxide. In order to separate glutamate from glutamine, the amino acid mixture was passed through a 3 cm^3 Dowex-1 (acetate) column and then collected with 15 ml 0.5 N acetic acid. The glutamate fraction from the culture medium was converted to its trifluoroacetyl butyl ester (TAB) (Leimer et al. 1977). Under EI conditions, ionization of TAB-glutamate produces two fragments, *m/z* 198 and *m/z* 152, corresponding to C2–C5 and C2–C4 of glutamate. Glutamate labeled on the 4–5 carbon positions indicates pyruvate dehydrogenase activity, while glutamate labeled on the 2–3 carbon positions indicates pyruvate carboxylase activity for the entry of glucose carbons to the TCA cycle. TCA cycle anabolic glucose utilization is calculated based on the m_1/m_2 ratios of glutamate (Lee et al. 1996).

15.3 Lipid Extraction and Analysis

Lipid extractions were performed using methods described elsewhere (Lowenstein et al. 1975). In brief, the Trizol extracts (bottom layer) of cell pellets after RNA extraction were saponified with 500 μl of 30 % KOH-ethanol (1:1 v/v) at 70 °C overnight. The aqueous phase was acidified, and fatty acids were extracted in petroleum ether and dried under a stream of nitrogen. Fatty acids were methylated with 0.5 ml 0.5 N HCl in methanol for GC/MS analysis. Palmitate, stearate, and

oleate were monitored at *m/z* 270, *m/z* 298, and *m/z* 264, respectively, with the enrichment of ^{13}C-labeled acetyl units either from tracer-labeled glucose or stearate, which reflect synthesis, elongation, and desaturation of the new lipid fraction as determined by mass isotopomer distribution analysis (MIDA) of different isotopomers (Lee et al. 1991). Mass isotopomer distribution was determined using the method of Lee et al., which corrects for the contribution of derivatizing agent and ^{13}C natural abundance to the mass isotopomer distribution of the compound of interest. The calculated mass isotopomer distribution is expressed as molar fractions (m_0, m_1, m_2, m_3, etc.), which are the fractions of molecules containing 0, 1, 2, 3, etc. ^{13}C substitutions, respectively. Data reduction and regression analyses were performed using the computer software Microsoft Excel® version 5.0.

Determination of Precursor Enrichment β-oxidation of [U-$^{13}C_{18}$]-stearate generates [1,2-$^{13}C_2$]acetyl-CoA, which is subsequently used as a precursor for de novo lipogenesis, chain elongation, energy production, and anaplerosis via the tricarboxylic acid cycle. Thus, β-oxidation can be assessed through the determination of [1,2-$^{13}C_2$]acetyl-CoA enrichment in the different synthetic products.

Acetyl-CoA Enrichment for De Novo Synthesis from Glucose The enrichment of the cytosolic acetyl-CoA pool used in de novo fatty acid synthesis was determined from the mass isotopomer distribution in palmitate and stearate using the [1,2-$^{13}C_2$]-D-glucose as the tracer. De novo synthesis produces these long-chain saturated fatty acids with 2, 4, or 6 ^{13}C atoms (m_2, m_4, and m_6). The distribution of these mass isotopomers has been previously shown to be a binomial distribution (Lee et al. 1992; Hellerstein 1991). Thus, the acetyl-CoA enrichment may be obtained from the consecutive mass isotopomer ratio $m_4/m_2 = (n-1)p/q = 3.5p/q$, where n is the number of acetyl units in palmitate = 8, p is the enrichment of [1,2-$^{13}C_2$]acetyl-CoA, q is the unenriched acetyl-CoA, and $p + q = 1$.

Acetyl-CoA Enrichment from Mitochondrial Oxidation: [1,2-$^{13}C_2$]acetyl-CoA produced either from [1,2-$^{13}C_2$]-D-glucose or [U-$^{13}C_{18}$]-stearate from β-oxidation combines with oxaloacetic acid and forms citric acid in the mitochondria. Citrate participates in the tricarboxylic acid cycle, eventually forming [α-4,5-$^{13}C_2$] ketoglutarate and glutamate (Haber et al. 2001). The enrichment of the m_2 component of the C2–C5 fragment generally reflects tricarboxylic acid cycle activity. However, it is well known that contribution from unlabeled glutamate from the cells in culture with glutamine-containing medium can substantially dilute the glutamate enrichment (Darmaun et al. 1988). Therefore, the enrichment of the [4,5-$^{13}C_2$]glutamate reflects the lower limit of mitochondrial acetyl-CoA cycling and anaplerosis.

Acetyl-CoA Enrichment for Chain Elongation Enzymes involved in chain elongation from [U-$^{13}C_{18}$]-stearate to longer-chain fatty acids are located in the endoplasmic reticulum, mitochondria, and peroxisomes (Vance et al. 2002). Chain elongation of uniformly labeled stearate with [1,2-$^{13}C_2$]acetyl-CoA produces characteristic m+18 clusters that can be used to determine the acetyl-CoA enrichment

according to the rules of combination of two labeled precursors. The ratio of m+2 to m+0 acetyl-CoA for chain elongation is given by the ratio of m+20 to m+18 in arachidate using the [U-$^{13}C_{18}$]-stearate tracer. The enrichment of [1,2-$^{13}C_2$]acetyl-CoA for each step of chain elongation was determined using the method described elsewhere using HepG2 cells as the in vitro model of fatty acid metabolism in the presence of [U-$^{13}C_{18}$]-stearic acid (Wong et al. 2004).

15.4 Gas Chromatography/Mass Spectrometry (GC/MS)

Mass spectral data were obtained on the HP5973 mass-selective detector connected to an HP6890 gas chromatograph. The settings were as follows: GC inlet 250 °C, transfer line 280 °C, MS source 230 °C, and MS Quad 150 °C. An HP-5 capillary column (30 m length, 250 μm diameter, 0.25 μm film thickness) was used for glucose, ribose, deoxyribose, glutamate, and lactate analyses. Alternatively, a Bpx70 column (25 m length, 220 μm diameter, 0.25 μm film thickness, SGE Incorporated, Austin, TX) was used for fatty acid analysis with specific temperature programming for myristate (C:14), palmitate (C:16), stearate (C:18), oleate (C:18-1), as well as C:20, C:22, and C:24 fatty acid analyses.

15.5 Data Analysis and Statistical Methods

Each experiment was carried out using triplicate cell cultures for each condition within each experiment, and experiments were repeated once. Mass spectroscopic analyses were carried out by three independent automatic injections of 1 μl samples by the automatic sampler and accepted only if the standard sample deviation was less than 1 % of the normalized peak intensity. Statistical analysis was performed using the Student's t-test for unpaired samples. With two-tailed significance at the 99 % confidence interval ($\mu \pm 2.58\sigma$), $P < 0.01$ indicated significant differences in glucose carbon metabolism in control and rosiglitazone-treated HepG2 cells. SIDMAParray™ was produced by MeTa-Informatics (San Diego, CA). Please see additional method references in doi: 10.1007/s11306-006-0015-5.

Acknowledgments Isotopolome-wide mathematical fitting of GC-MS data involving ^{13}C-glucose with ^{13}C-stearate to product processing was supported by the Hirshberg Foundation for Pancreatic Cancer Research and the UCLA Clinical and Translational Science Institute (UL1TR000124) to LGB and EJM. Targeted ^{13}C tracer drug efficacy marker data diagnostics for cancer were partially supported by the European Regional Development Fund, Central Hungary Operative Program, and New Széchenyi Plan (KMOP-1.1.4-11/A-2011-01-05) to GS. We thank Eszter Boros and Ferenc Nádudvari for their technical help in registering additional ^{13}C tracer presentation by LGB on the World Wide Web at http://youtu.be/GkYAjabGxJs regarding mammalian cell mitochondria.

Conflict of Interest The authors declare no conflict of financial interest.

Disclaimer The views presented in this article do not necessarily reflect those of the Food and Drug Administration (FDA) of the United States of America.

References

Beger RD, Colatsky T (2011) Metabolomics data and the biomarker qualification process. Metabolomics 8:2–7

Beger RD et al (2009) Single valproic acid treatment inhibits glycogen and RNA ribose turnover while disrupting glucose-derived cholesterol synthesis in liver as revealed by the [U-$^{13}C_6$]-D-glucose tracer in mice. Metabolomics 5:336–345

Boros LG, Cascante M, Lee WN (2002) Metabolic profiling of cell growth and death in cancer: applications in drug discovery. Drug Discov Today 7:364–372

Boros LG, Serkova NJ, Laderoute KR, Linehan WM, Meuillet MJ (2013) Stable ^{13}C isotope enriched metabolome (isotopolome) wide associations (IWAS) improve system wide association studies (SWAS) for phenotype and drug research. World Biotechnology Congress 4:A29, SL-31. http://www.worldbiotechcongress.com/files/Abstract-Book-GBC-(2013).pdf

Chang CH, Lin JW, Wu LC, Lai MS, Chuang LM, Chan KA (2012) Association of thiazolidinediones with liver cancer and colorectal cancer in type 2 diabetes mellitus. Hepatology 55:1462–72. doi:10.1002/hep.25509

Darmaun D, Matthews DE, Desjeux JF, Bier DM (1988) Glutamine and glutamate nitrogen exchangeable pools in cultured fibroblasts: a stable isotope study. J Cell Physiol 134:143–148

Haber S, Lapidot A (2001) Energy fuel utilization by fetal versus young rabbit brain: a 13C MRS isotopomer analysis of [U-13C6]glucose metabolites. Brain Res 896:102–117

Harrigan GG, Colca JR, Szalma S, Boros LG (2006) PNU-91325 increases fatty acid synthesis from glucose and mitochondrial long chain fatty acid degradation: a comparative tracer-based metabolomics study with rosiglitazone and pioglitazone in HepG2 cells. Metabolomics 2:21–29. doi:10.1007/s11306-006-0015-5

Hellerstein MK (1991) Relationship between precursor enrichment and ratio of excess M2/excess M1 isotopomer frequencies in a secreted polymer. J Biol Chem 266:10920–10924

Holleran AL, Briscoe DA, Fiskum G, Kelleher JK (1995) Glutamine metabolism in AS-30D hepatoma cells. Evidence for its conversion into lipids via reductive carboxylation. Mol Cell Biochem 152:95–101

Katz J, Wals P, Lee WN (1993) Isotopomer studies of gluconeogenesis and the Krebs cycle with 13C-labeled lactate. J Biol Chem 268:25509–25521

Lee WN, Bergner EA, Guo ZK (1992) Mass isotopomer pattern and precursor-product relationship. Biol Mass Spectrom 21:114–122

Lee WN, Edmond J, Bassilian S, Morrow JW (1996) Mass isotopomer study of glutamine oxidation and synthesis in primary culture of astrocytes. Dev Neurosci 18:469–477

Lee WN, Lim S, Bassilian S, Bergner EA, Edmond J (1998a) Fatty acid cycling in human hepatoma cells and the effects of troglitazone. J Biol Chem 273:20929–20934

Lee WN, Boros LG, Puigjaner J, Bassilian S, Lim S, Cascante M (1998b) Mass isotopomer study of the nonoxidative pathways of the pentose cycle with [1,2-13C2]glucose. Am J Physiol 274: E843–E851

Leimer KR, Rice RH, Gehrke CW (1977) Complete mass spectra of N-trifluoroacetyl-n-butyl esters of amino acids. J Chromatogr 141:121–144

Lowenstein JM, Brunengraber H, Wadke M (1975) Measurement of rates of lipogenesis with deuterated and tritiated water. Methods Enzymol 35:279–287

Metallo CM, Walther JL, Stephanopoulos GJ (2009) Evaluation of ^{13}C isotopic tracers for metabolic flux analysis in mammalian cells. J Biotechnol 144:167–174. doi:10.1016/j.ymben.2011.12.004

Mullen AR, Wheaton WW, Jin ES, Chen PH, Sullivan LB, Cheng T, Yang Y, Linehan WM, Chandel NS, DeBerardinis RJ (2011) Reductive carboxylation supports growth in tumour cells with defective mitochondria. Nature 481:385–388

Otto C, Lehrke M, Goke B (2002) Novel insulin sensitizers: pharmacogenomic aspects. Pharmacogenomics 3:99–116

Sabate L, Franco R, Canela EI, Centelles JJ, Cascante M (1995) A model of the pentose phosphate pathway in rat liver cells. Mol Cell Biochem 142:9–17

Son J, Lyssiotis CA, Ying H, Wang X, Hua S, Ligorio M, Perera RM, Ferrone CR, Mullarky E, Shyh-Chang N, Kang Y, Fleming JB, Bardeesy N, Asara JM, Haigis MC, DePinho RA, Cantley LC, Kimmelman AC (2013) Glutamine supports pancreatic cancer growth through a KRAS-regulated metabolic pathway. Nature 496:101–105. doi:10.1038/nature12040

Sonko BJ, Schmitt TC, Guo L, Shi Q, Boros LG, Leakey JE, Beger RD (2011) Assessment of usnic acid toxicity in rat primary hepatocytes using ^{13}C isotopomer distribution analysis of lactate, glutamate and glucose. Food Chem Toxicol 49:2968–2974

Vance DE, Vance KE (2002) Biochemistry of lipids, lipoproteins and membranes, 4th edn. Elsevier Science, New York, pp 183–187

Vamecq J, Colet J-M, Vanden Eynde JJ, Briand G, Porchet N, Rocchi S (2012) PPARs: interference with Warburg' effect and clinical anticancer trials. PPAR Res Article ID 304760

Walther JL, Metallo CM, Zhang J, Stephanopoulos G (2012) Optimization of ^{13}C isotopic tracers for metabolic flux analysis in mammalian cells. Metab Eng 14:162–171

Wong DA, Bassilian S, Lim S, Lee WN (2004) Coordination of peroxisomal beta-oxidation and fatty acid elongation in HepG2 cells. J Biol Chem 279:41302–41309

Yang Y, Lane AN, Ricketts C, Wei M-H, Pike L, Wu M, Rouault TA, Boros LG, Fan TW-M, Linehan WM (2013) Metabolic reprogramming for producing energy and reducing power in Fumarate Hydratase null cells from hereditary leiomyomatosis renal cell carcinoma. PLoS One 8:e72179. doi:10.1371/journal.pone.0072179